Optimizing WRF as a regional climate Downscaling Tool for Hydro-climatological Applications in the Eastern Nile Basin

Mahmoud Osman[a]*

George Zittis[b]

Mohammed AbouElHaggag[a]

Ahmad W. Abdeldayem[a]

Jos Lelieveld[b,c]

[a] *Faculty of Engineering, Cairo University, Giza, Egypt.*

E-mail: mosman@cu.edu.eg; mosman7@jhu.edu; *Tel. +1(970)412-7545*

[b] *The Cyprus Institute, Nicosia, Cyprus.*

[c] *Max Planck Institute for Chemistry, Mainz, Germany.*

This study contributes to the development of an integrated hydro-climate model for the EN basin for the impact assessment of the Nile inflow at Aswan by configuring a RCM using WRF to downscale ERA-Interim reanalysis data from 1980 to 2009 and correct the resulted model bias.

Keywords:

Dynamic downscaling; Bias correction; Eastern Nile Basin; WRF; Precipitation patterns

1. Abstract:

Most of the Nile water inflow at High Aswan Dam (HAD), Egypt, originates from the Ethiopian plateau, providing the main source of water for the Eastern Nile (EN) basin. The Weather Research and Forecasting (WRF) model using ARW (Advanced Research WRF) dynamical core is configured for a domain centered over the EN with a parent domain defined for the Middle East – North Africa (MENA). WRF physics parameterization sensitivity experiments are carried out to select an optimum combination of physics schemes to reproduce observed climate conditions. The model skill is also examined by downscaling the ERA-Interim reanalysis dataset from 1980 to 2009 over the EN basin domain. The WRF performance is assessed using gridded observational datasets for precipitation, temperature and evapotranspiration. The model is tested for four different configurations in two-year simulations to determine the optimal combination of physics parameterizations prior to the 30-year downscaling experiment. The results indicate accurately modelled temperature and evapotranspiration fields, however, with significant positive precipitation biases, especially over the highlands. The bias-corrected precipitation data is coupled to the semi-distributed hydrological rainfall-runoff model (SWAT) model, previously configured for the Baro-Akobo-Sobat sub-basin. The simulated flow hydrograph based on bias-corrected WRF simulations yields high statistical significance for the observed flow hydrographs. Results indicate that the simulated precipitation fields from WRF should be subject to bias correction prior to use in hydrological models especially for impact studies.

2. Introduction

Throughout the last three decades, global and regional climate models have been developed and widely utilized to project future climate conditions, and to help better understand the present and past climate [6,10,26,31]. Dynamic downscaling techniques can be applied to bring global-scale projections down to a regional level where the output of general circulation models (GCMs) provides the initial and boundary conditions. Considerable computing resources are involved, where high resolution climate scenarios provided by regional climate models (RCMs) allow for a more precise description of topographic forcing due to orography, land-sea contrasts and land-use characteristics [11,17,20]. In this study, we use the Weather Research and Forecasting Model (WRF) version 3.5, which is used by more than 30,000 researchers in excess of 150 countries, and allows researchers to generate atmospheric simulations based on real data (observations, reanalysis) or idealized conditions (http://www.wrf-model.org).

Assessments of the future climate in the Eastern Nile Basin (EN) basin are still limited and the level of understanding of future climate behavior is not yet clear to the different decision makers and stakeholders in the EN. This is mainly because of the complexity of carrying out representative climate studies. The complexity and chaotic nature of the climate system suggest that future climate conditions cannot be represented by simply extrapolating past climate conditions. Instead, mathematical representations of the Earth's climate system through high resolution RCM the accounts for the region's climatic physics.

This study pursues a high-resolution RCM for the EN basin that is configured and bias corrected based on a 30-year simulation period (from 1980 to 2009) and serving hydro-climatological applications.

There is a paucity in the relevant research studies that assess the performance of the WRF model over the Nile basin and specifically over the EN basin. Few studies [1,5,14,37,44] focused on the impacts of climate change on the hydrology at different regions in the Nile basin hydrology and Lake Victoria basin using WRF dynamic downscaling and statistical downscaling techniques. The objective of our study is to fill the gap in the EN basin region by optimizing the WRF for dynamic downscaling instead of using the classical statistical downscaling techniques as well as studying the generated bias from the model hydrodynamics. The results of the study are expected to be used in future dynamic downscaling of climate models for hydro-climatological applications using pre-configured WRF model. The model is configured for the simulations using the WRF-ARW (Advanced Research WRF) dynamical core developed at the National Center for Atmospheric Research (NCAR) [38].

3. Materials and Methods

2.1. Region of Study

The EN hydrologic boundaries extend from the Ethiopian Highlands (~3°N) in the south to the High Aswan Dam (HAD) in the North (~24°N) and from the west of Sudan (~26° E) to the Gulf of Aden (~42° E) as shown in Figure 1. Elevations in the EN basin range from 0 to 4,300 meters above mean sea level. About 5% of the basin lies in very low elevated areas while most of the EN (around 70%) is situated within the range of 300 - 600 m. Another 20% is between 600 - 2000 m and the remaining 5% is associated with very steep slopes (around 2000 m - 4300 m) [41]. Ethiopia has a general elevation ranging from 1,500 to 3,000 m and the plateau height exceeds 4,000 m. A key land feature in Ethiopia is Lake Tana, created by volcanic activity, at a height of 1,785 m. In Sudan, elevations vary between 170 m and 1,475 m whereas in South Sudan, elevation ranges from 380 m to 2,885 m [3,34,37,41]

The EN is divided into five sub-basins that include the Main Nile, the Baro-Akobo-Sobat,-White Nile, the Abay-Blue Nile, and the Tekeze-Atbara-Setite. The Abay-Blue Nile and the Main Nile region host nearly 82% of the total population [13,37].

Precipitation over the Nile basin increases from the north to the south (with elevation) with values up to 1,600 mm/year over the Ethiopian highlands, which is mainly governed by the interaction with the basin topography and the Inter-Tropical Convergence Zone movement [32,41].

2.2. Methodology

The methodology applied for hydro-climatic simulations and dynamical climate downscaling over the EN basin is summarized in the flow chart of Figure 2. The regional climate modeling is carried out using version 3.5 of the WRF model over a domain covering the Middle East and North Africa (MENA) including the EN region. Climate downscaling is performed by forcing the WRF model with initial and boundary conditions from the European Centre for Medium-Range Weather Forecast (ECMWF) ERA-Interim reanalysis dataset [4], in order to (a) select the suitable combination of physics parameterizations and (b) investigate the model skill in reproducing the past and present climate conditions. The model is configured as sub-domain (nest) in the Coordinated Regional Climate Downscaling Experiment (CORDEX)-MENA domain, encompassing 185 x 250 horizontal grid points (~10km grid resolution) and 30 vertical grid levels as shown in Figure 3. The integration timestep is set to 240 seconds for the MENA parent domain computations and 1:5 as parent to nest timestep ratio which is the same ratio used for nesting the EN domain. The spin-up time is set to seven months after sensitivity analysis to model for different spin-up periods.

Because the CORDEX domain is large and parts of it are out of context for the EN region we focus our evaluation only on the high-resolution nest and the 12 sub-domains listed in Table 2 that represent the individual watersheds of the EN and cover different climatic zones up to the High Aswan Dam. The selected regions are equally sized as boxes of dimensions 2° by 2° represented in Figure 1. Each of them covers approximately 484 grid points at the EN domain selected resolution.

2.3 Sensitivity to Physics Parameterization

Based on previous study of the CORDEX MENA domain [45,46] and following other physics sensitivity studies [7,15,18,19,24,27,28,33,36,39], four physics combinations, commonly used for regional climate simulations, are used to test the model sensitivity towards different parameterization schemes (Table 1). The physics representations were tested for precipitation and temperature over two years of extreme different precipitation regimes over the Nile basin; 1999 as a wet year and 1984 as a dry year [37].

As reference data for the model evaluation we use the Global Precipitation Climatology Center (GPCC) dataset [35] for precipitation, while the UDEL [43] is used for temperature. The Pearson’s correlation coefficient (COR) is used to determine the skill of the model to simulate the variables pattern across the simulation period (Equation 2-1), the Root Mean Square Error (RMSE), (Equation 2-2) and the Mean Absolute Error (MAE), (Equation 2-3) are also calculated to assess the quality of the model and estimate model simulation biases:

$$\boldsymbol{COR = \frac{cov(OBS, SIM)}{\sigma_{OBS} \cdot \sigma_{SIM}} = \frac{\sum_{i=1}^{n}(OBS_i - \overline{OBS})(SIM_i - \overline{SIM})}{\sigma_{OBS} \cdot \sigma_{SIM}}}$$

Equation 2-1

$$\boldsymbol{MAE = \frac{1}{n}\sum_{i=1}^{n} |\, SIM_i - OBS_i|}$$

Equation 2-2

$$\boldsymbol{RMSE = \sqrt{\frac{\sum_{i=1}^{n}(SIM_i - OBS_i)^2}{n}}}$$

Equation 2-3

Where n is the number of sample, and OBS and SIM are the observed and simulated variables.

2.4 Observational Datasets

Based on availability throughout the study period (1980-2009), spatial resolution and quality of data, the following sets are selected:

- The GPCC dataset version 6.0, covering the period 1901 to 2010, contains monthly precipitation sums and has a spatial resolution of 0.5° × 0.5° latitude by longitude [35].

- The University of Delaware (UDEL) monthly global dataset for air temperature and precipitation from 1950 to 2010 with as spatial resolution of 0.5° × 0.5° latitude by longitude [43].

- The NCEP-LHF high resolution monthly mean global reanalysis dataset of the latent heat flux, used as a proxy of evapotranspiration. The dataset is available from 1901 to 2015 at a spatial horizontal resolution 0.3° × 0.3° latitude by longitude [25].

4. Results and Discussion

We performed a Taylor diagram-based statistical analysis for the four model configurations by comparing with the UDEL dataset for the monthly average temperature in 1999 and 1984. The analysis shows no significant difference between the chosen physics packages, which indicates that the four parameterization groups behave similarly in simulating the temperature over the Eastern Nile Basin (Figure 4 - A). Physic configurations 1 and 4 show nearly similar performance for both precipitation and temperature for the selected two years (Figure 4 - B). However, as an overall an equally weighted average for the RMSE and COR parameters for the selected 12 regions in the years 1984 and 1999, the performance of physics configuration “4” was found to give slightly better results (Table 3) and is selected for the historical 30 years downscaling experiment and includes “Lin” [9] Microphysics scheme, “MYJ” [22] Planetary boundary layer parameterization scheme, “BMJ” Cumulus scheme [23], “CAM” [12] radiation scheme and “NOAH” [8] land surface model.

3.1 Evapotranspiration

The latent heat flux at the surface is a WRF output variable that can be used as an indicator of evapotranspiration in terms of energy flux. The results of the model are compared with the observational dataset NCEP-LHF for the 30-year simulation period from 1980 to 2009 to estimate the model bias shown in Figure 5, i.e. after conversion to the conventional evapotranspiration unit (mm/day) using Equation 4-1. The model shows high precision in simulating evapotranspiration in the region, with a relatively small bias that generally does not exceed 0.5 mm/day.

$$ET=\frac{LHF}{L_v} \qquad \textbf{Equation 3-1}$$

where *ET* is the evapotranspiration in (mm/day), *LHF* is the latent heat flux in (W/m^2), L_v is the latent heat of vaporization for water in (J/Kg).

3.2 Temperature

The 2-meter mean temperature over the 12 analysis sub-regions (Figure 6) shows a very high correlation to the UDEL observational dataset. Figure 7-A also depicts the relatively small temperature biases (±1°C), as expected [21,30], indicating that the simulated temperature is adequate for the hydrologic applications.

3.3 Precipitation

Precipitation results from WRF are still highly uncertain due to the complexity of cloud formation and the precipitation physics representation. The model appears to overestimate precipitation over the highlands and underestimates it in low elevation regions, which needs further validation for application in hydrologic applications. Figure 7-B shows the bias of the daily average over the 30-year period from 1980 to 2009.

The bias in precipitation is evident in the comparison for sub-regions, showing an underestimation in most of the dry parts and overestimation in the highlands, while both overestimation and underestimation were noticed in some regions like in Obeid. Figure 8 illustrate the modeled precipitation over three regions (Akobo, BN and GERD) out of the 12-selected analysis zones as time series of monthly precipitation (figures for other regions are not shown), averaged over all grid points of each sub-region. Interestingly, substantial differences between the monthly precipitations of the two gridded observational datasets are also found. This underscores concerns regarding the uncertainty in observational data sets [40].

The modeled precipitation is still subject to bias correction due to the obvious bias in modeling the past/present compared to the GPCC and UDEL datasets. The following sections will discuss in detail the correction methods followed, and the hydrologic verification technique to assure the adequacy of the chosen correction method [16].

3.4 Precipitation Bias Correction

Several bias correction methods have been proposed, focusing mainly on precipitation and temperature. In view of the intricacy of physical processes to simulate precipitation, there are different methods at different levels of complexity available, from simple linear methods to empirical or theoretical functions aiming to correct moments of precipitation distribution [2].

Following a wide variety of bias correction methods [2], the algorithm followed to correct the precipitation output of our climate simulations is based on verifying the adjusted rainfall rates by applying them to a semi distributed Rainfall-Runoff hydrological model (SWAT) and assessing the quality of the output flow hydrograph compared to that observed.

The aim is to ensure the adequacy of the corrected precipitation results for hydrologic applications.

The selected study region for the SWAT model is the Gambella watershed, which is a part of the Baro-Akobo-Sobat Sub-Basin of the EN as shown in Figure 9. The Gambella watershed covers an area of approximately 23,450 km^2 over a wide elevation range, i.e. from a minimum of 450 m to a maximum of 2,650 m. The watershed is calibrated using ground-based observations of the runoff available near the streams in a previous study [34]. The weather information used was from the global GHCN dataset version 2. After calibration, the model has shown a very high coefficient of determination (R^2) value of nearly 0.95, and a Nash-Sutcliffe Efficiency value (NSE) of 0.92.

The *First* bias-correction method is based on the probability distribution of the average monthly precipitation in the whole domain [29]. The monthly GPCC precipitation is found to be best fitted as Weibull distribution with a maximum likelihood method, and shape and scale factors equal to 1.279 and 1.545, respectively, as shown in Figure 10 -A, while the modeled precipitation has shape and scale factors equal to 1.202 and 1.183, respectively, as shown in Figure 10 - B.

We find that the WRF simulated precipitation, i.e. according to the distribution parameters, is underestimated by 30% compared to the observations, which is demonstrated in the Q-Q plot of Figure 11 - A. The simulated precipitation is corrected by regressing the simulated precipitation against the observation, resulting in a multiplicative constant so that the Weibull distribution of the WRF precipitation becomes 1.242 and 1.539 for the shape and scale factors, respectively, resulting in improved representation of the simulated precipitation, and matching the observed GPCC precipitation over the EN region. The Q-Q plot of the bias-corrected precipitation, shown in Figure 11 – B, gives the best representation of the observations in the 30 years study period based on the probability distribution method.

The resulting bias-corrected precipitation is used as input for the SWAT hydrological model for the Gambella watershed for verification. The runoff results of the hydrological model shown in Figure 12-A yield a very high coefficient of determination (R^2=0.88), while the values are highly overestimated according to the Nash-Sutcliffe Efficiency, about -0.15, which is not acceptable for hydrological models. The bias-correction method based on the probability distribution is therefore rejected for hydrological applications, even though the statistical parameters indicate good agreement with observations.

The *Second* correction method relies on inspection of the precipitation bias against the elevation in each grid as shown in Figure 13. The elevation contour lines are plotted over the precipitation bias map for the 30-year period from 1980 to 2009. The bias is correlated to the terrain elevation, notably over the ETH, such that the bias-correction algorithm is a function of location and terrain elevation.

The bias-correction matrices are divided into five bands based on elevation ranges, with band 1 representing the bias for grid points with elevation less than 500 m, band 2 from 500 to 1,000 m, band 3 from 1,000 to 1,500 m, band 4 from 1,500 to 2,000 m and band 5 for grids of altitude more than 2,000 m as shown in Figure 14.

The bias is corrected using the GPCC dataset and applied to the WRF model output at a condition that zero is the minimum value of precipitation. The resulting bias-corrected precipitation is again coupled with the SWAT hydrological model for the Gambella watershed. The runoff results of the hydrological model shown in Figure 12-B also yield a high coefficient of determination (R^2=0.80) and a good Nash-Sutcliffe Efficiency of ~0.61, which is considered sufficient for hydrological models.

The *Third* tested correction method is based on finding the relation between bias and the time of the year as a repeating cycle throughout the considered period, with the same bias for the same month, e.g. the monthly daily average precipitation bias from observations in

January 1980 was almost the same as in January 1981, 1982 … etc. The algorithm of correction depends on the daily average bias relative to the GPCC data in the same month, across the year for each grid in the domain. Figure 15 depicts the generated 12 bias-correction matrices as daily average bias in each month. It is clear that the bias in August is largest, with an underestimation of more than 10 mm/day, and smallest in May, July and October, with almost no precipitation prediction bias.

The-bias corrected precipitation is again coupled to the SWAT model for the Gambella watershed to assess the correction method against the previous two methods. The runoff results of the hydrological model, shown in Figure 12-C, yield a very high coefficient of determination (R^2=0.86), and a very good Nash-Sutcliffe Efficiency (NSE) of ~0.79, which is considered excellent for hydrological models.

Hence, the three bias correction methods applied here resulted in statistically acceptable results (overall mean and standard deviation of the modeled precipitation), however, verification based on a hydrological model the results for runoff were different. The time-location method was found to be the best bias-correction method, which should be applied to the modeled precipitation output for use in hydrologic applications.

5. Conclusions

The WRF model appears to be able to achieve high precision in simulating both temperature and evapotranspiration, with minor biases and errors based on the comparison with the observational datasets. However, precipitation is less accurately simulated, and the results need to be subject to bias correction to insure their validity for hydrologic applications.

The three bias-correction methods applied to WRF simulated precipitation output perform differently when compared to the rainfall-runoff hydrological model results. The Time-Location method, assuming a repeating monthly bias cycle throughout the years over the period considered appears to yield optimal performance, producing a valid precipitation product for the EN region at a high resolution, appropriate for hydrologic applications. The Time-Location method improved the NSE value of the runoff results using the WRF corrected precipitation from -0.15 for the probability distribution correction method to 0.79, as well as preserving the high coefficient of determination R^2 value around 0.86.

Hydrological verification of the bias-correction method is found to be an essential step in approving the correction method, since the results need to be used in hydrologic applications. Further, our results with the WRF model give confidence that scenario calculations will be useful for the future projection of temperature, evapotranspiration and precipitation, the latter at the condition of considering bias-correction with the proposed algorithm (Time-Location Method). The success of this method also underscores the weakness of climate models in reproducing rainfall in regions with pronounced topography.

6. Acknowledgments

Sincere acknowledgements are due to Cairo University, The Cyprus Institute and Max Plank Institute for Chemistry. Special acknowledgement is due to CORDEX for support through training, computational resources and the professional technical assistance.

7. References and Citations:

1. Argent, R. E. (2014). *Customization of the WRF Model Over the lake Victoria Basin in East Africa*. North Carolina State University.
2. Argüeso, D., Evans, J. P., & Fita, L. (2013). Precipitation bias correction of very high resolution regional climate models. *Hydrology and Earth System Sciences*, *17*(11), 4379–4388. http://doi.org/10.5194/hess-17-4379-2013
3. Asore. (2012). *Impact of climate change on potential evapotranspiration and runoff in the Awash River basin in Ethiopia*. Cairo University.

4. Berrisford, P., Dee, D. P., Poli, P., Brugge, R., Fielding, K., Fuentes, M., Simmons, A. (2011, November). The ERA-Interim archive Version 2.0. *ERA Report Series*. Shinfield Park, Reading: ECMWF.
5. Beyene, T., Lettenmaier, D. P., & Kabat, P. (2010). Hydrologic impacts of climate change on the Nile River Basin: implications of the 2007 IPCC scenarios. *Climatic Change*, *100*(3–4), 433–461. http://doi.org/10.1007/s10584-009-9693-0
6. Buontempo, C., Mathison, C., Jones, R., Williams, K., Wang, C., & McSweeney, C. (2015). An ensemble climate projection for Africa. *Climate Dynamics*, *44*(7–8), 2097–2118. http://doi.org/10.1007/s00382-014-2286-2
7. Caldwell, P., Chin, H. N. S., Bader, D. C., & Bala, G. (2009). Evaluation of a WRF dynamical downscaling simulation over California. *Climatic Change*, *95*(3–4), 499–521. http://doi.org/10.1007/s10584-009-9583-5
8. Chen, F., Mitchell, K., Schaake, J., Xue, Y., Pan, H.-L., Koren, V., Betts, A. (1996). Modeling of land surface evaporation by four schemes and comparison with FIFE observations. *Journal of Geophysical Research*, *101*(D3), 7251. http://doi.org/10.1029/95JD02165
9. Chen, S.-H., & Sun, W.-Y. (2002). A One-dimensional Time Dependent Cloud Model. *Journal of the Meteorological Society of Japan*, *80*(1), 99–118. http://doi.org/10.2151/jmsj.80.99
10. Clarke, L. E., Jacoby, H., Pitcher, H., Reilly, J., & Richels, R. (2007). Scenarios of Greenhouse Gas Emissions and Atmospheric, (July), 154.
11. Cohen, S. J. (1990). Bringing the Global Warming Issue Closer to Home: The Challenge Of Regional Impact Studies. *Bulletin of the American Meteorological Society*. http://doi.org/10.1175/1520-0477(1990)071<0520:BTGWIC>2.0.CO;2

12. Collins, W. D., Rasch, P. J., Boville, B. A., Hack, J. J., McCaa, J. R., Williamson, D. L., Zhang, M. (2006). The formulation and atmospheric simulation of the Community Atmosphere Model version 3 (CAM3). *Journal of Climate*, *19*(11), 2144–2161. http://doi.org/10.1175/JCLI3760.1
13. DHI. (2006). *DHI product suite: Set of manuals: Water Atlas of the Blue Nile Sub-Basin*. Denmark.
14. Di Baldassarre, G., Elshamy, M., van Griensven, A., Soliman, E., Kigobe, M., Ndomba, P., Uhlenbrook, S. (2011). Future hydrology and climate in the River Nile basin: a review. *Hydrological Sciences Journal*, *56*(2), 199–211. http://doi.org/10.1080/02626667.2011.557378
15. Done, J. M., Leung, L. R., Davis, C. A., & Kuo, B. (2005). Regional Climate Simulation Using the WRF Model . In *WRF/MM5 User's Workshop*.
16. Elshamy, M. E., Seierstad, I. A., & Sorteberg, A. (2009). Impacts of climate change on Blue Nile flows using bias-corrected GCM scenarios. *Hydrology and Earth System Sciences*, *13*(5), 551–565. http://doi.org/10.5194/hess-13-551-2009
17. Evans, J. P. (2012). Regional Climate Modelling: The Future for Climate Change Impacts and Adaptation Research. Retrieved April 5, 2016, from http://www.earthzine.org/2012/02/14/regional-climate-modelling-the-future-for-climate-change-impacts-and-adaptation-research/
18. Fujino, J., Nair, R., Kainuma, M., Masui, T., & Matsuoka, Y. (2006). Multi-gas Mitigation Analysis on Stabilization Scenarios Using Aim Global Model. *The Energy Journal*, *27*, 343–353. Retrieved from http://www.jstor.org/stable/23297089
19. Gbobaniyi, E., Sarr, A., Sylla, M. B., Diallo, I., Lennard, C., Dosio, A., Lamptey, B. (2014). Climatology, annual cycle and interannual variability of precipitation and

temperature in CORDEX simulations over West Africa. *International Journal of Climatology*, *34*(7), 2241–2257. http://doi.org/10.1002/joc.3834

20. Giorgi, F. (1990). Simulation of Regional Climate Using a Limited Area Model Nested in a General Circulation Model. *Journal of Climate*, *3*(9), 941–963. http://doi.org/10.1175/1520-0442(1990)003<0941:SORCUA>2.0.CO;2

21. IPCC. (2013). *CLIMATE CHANGE 2013 - They Physical Science Basis - Frequently Asked Questions*. *CLIMATE CHANGE 2013 - They Physical Science Basis*.

22. Janjić, Z. I. (1990). The Step-Mountain Coordinate: Physical Package. *Monthly Weather Review*, *118*(7), 1429–1443. http://doi.org/10.1175/1520-0493(1990)118<1429:TSMCPP>2.0.CO;2

23. Janjić, Z. I. (1994). The Step-Mountain Eta Coordinate Model: Further Developments of the Convection, Viscous Sublayer, and Turbulence Closure Schemes. *Monthly Weather Review*, *122*(5), 927–945. http://doi.org/10.1175/1520-0493(1994)122<0927:TSMECM>2.0.CO;2

24. Jin, J., Miller, N. L., & Schlegel, N. (2010). Sensitivity Study of Four Land Surface Schemes in the WRF Model. *Advances in Meteorology*, *2010*(November), 1–11. http://doi.org/10.1155/2010/167436

25. Kalnay, E., Kanamitsu, M., Kistler, R., Collins, W., Deaven, D., Gandin, L., Joseph, D. (1996). The NCEP/NCAR 40-Year Reanalysis Project. *Bulletin of the American Meteorological Society*, *77*(3), 437–471. http://doi.org/10.1175/1520-0477(1996)077<0437:TNYRP>2.0.CO;2

26. Kalognomou, E.-A., Lennard, C., Shongwe, M., Pinto, I., Favre, A., Kent, M., Büchner, M. (2013). A Diagnostic Evaluation of Precipitation in CORDEX Models over Southern Africa. *Journal of Climate*, *26*(23), 9477–9506.

http://doi.org/10.1175/JCLI-D-12-00703.1

27. Katragkou, E., García-Díez, M., Vautard, R., Sobolowski, S., Zanis, P., Alexandri, G., Jacob, D. (2015). Regional climate hindcast simulations within EURO-CORDEX: evaluation of a WRF multi-physics ensemble. *Geosci. Model Dev.*, *8*(3), 603–618. http://doi.org/10.5194/gmd-8-603-2015

28. Laprise, R., Hernández-Díaz, L., Tete, K., Sushama, L., Šeparović, L., Martynov, A., Valin, M. (2013). Climate projections over CORDEX Africa domain using the fifth-generation Canadian Regional Climate Model (CRCM5). *Climate Dynamics*, *41*(11–12), 3219–3246. http://doi.org/10.1007/s00382-012-1651-2

29. Legates, D. R., & McCabe, G. J. (1999). Evaluating the use of "goodness-of-fit" Measures in hydrologic and hydroclimatic model validation. *Water Resources Research*, *35*(1), 233–241. http://doi.org/10.1029/1998WR900018

30. Legates, D. R., & Willmott, C. J. (1990). Mean seasonal and spatial variability in global surface air temperature. *Theoretical and Applied Climatology*, *41*(1–2), 11–21. http://doi.org/10.1007/BF00866198

31. Lelieveld, J., Hadjinicolaou, P., Kostopoulou, E., Chenoweth, J., Maayar, M., Giannakopoulos, C., Xoplaki, E. (2012). Climate change and impacts in the Eastern Mediterranean and the Middle East. *Climatic Change*, *114*(3), 667–687. http://doi.org/10.1007/s10584-012-0418-4

32. Mohamed, Y. A., van den Hurk, B. J. J. M., Savenije, H. H. G., & Bastiaanssen, W. G. M. (2005). Hydroclimatology of the Nile: results from a regional climate model. *Hydrol. Earth Syst. Sci.*, *9*(3), 263–278. http://doi.org/10.5194/hess-9-263-2005

33. Otkin, J. A., H-L. Huang, and A. Seifert, (2006). A comparison of microphysical schemes in the WRF model during a severe weather event. In *7th Annual WRF User's*

Workshop. Boulder, CO, NCAR.

34. Raafat, A. (2015). *Assessment of the Impacts of Proposed Water Resources Development Projects in Baro-Akobo-Sobat Basin on HAD*. Cairo University.
35. Schamm, K., Ziese, M., Becker, A., Finger, P., Meyer-Christoffer, A., Schneider, U., Stender, P. (2014). Global gridded precipitation over land: a description of the new GPCC First Guess Daily product. *Earth Syst. Sci. Data*, *6*(1), 49–60. http://doi.org/10.5194/essd-6-49-2014
36. Shin, H. H., & Hong, S.-Y. (2011). Intercomparison of Planetary Boundary-Layer Parametrizations in the WRF Model for a Single Day from CASES-99. *Boundary-Layer Meteorology*, *139*(2), 261–281. http://doi.org/10.1007/s10546-010-9583-z
37. Siam, M. (2010). *Impact of Climate Change on the Upper Blue Nile Catchment Flows Using IPCC Scenarios*. Cairo University.
38. Skamarock, W.C. et al. 2008. “A Description of the Advanced Research WRF Version 3.” *Technical Report (June)*: 113.
39. Soares, P. M. M., Cardoso, R. M., Miranda, P. M. A., Medeiros, J., Belo-Pereira, M., & Espirito-Santo, F. (2012). WRF high resolution dynamical downscaling of ERA-Interim for Portugal. *Climate Dynamics*, *39*(9), 2497–2522. http://doi.org/10.1007/s00382-012-1315-2
40. Tanarhte, M., Hadjinicolaou, P., & Lelieveld, J. (2012). Intercomparison of temperature and precipitation data sets based on observations in the Mediterranean and the Middle East. *Journal of Geophysical Research: Atmospheres*, *117*(D12), http://doi.org/10.1029/2011JD017293
41. Tarabia, A. (2015). *Impact Assessment of the Proposed Water Resources Development Projects in the Blue Nile Basin on Nile Flow at Aswan*. Cairo

University.

42. Tesemma, Z. (2009). Long Term Hydrologic Trends in the Nile Basin, (May), 83.

43. UDel. (2015). UDel_AirT_Precip data. Boulder, CO: NOAA/OAR/ESRL PSD. Retrieved from http://www.esrl.noaa.gov/psd/

44. Weldemariam, H. G. (2015). *Dynamical Downscaling of GCM out puts to Determine Impacts of Climate Change and Variability on the Hydrologic Sensitivity of Blue Nile Basin Surface Water Resource Potential*. University of Nebraska.

45. Zittis, G., Hadjinicolaou, P., & Lelieveld, J. (2014). Comparison of WRF Model Physics Parameterizations over the MENA-CORDEX Domain. *American Journal of Climate Change*, *3*(5), 490–511. http://doi.org/10.4236/ajcc.2014.35042

46. Zittis, G., Hadjinicolaou, P., & Lelieveld, J. (2016). Performance of WRF as a regional climate model over the MENA-CORDEX domain; a comparison of two radiation schemes. *International Journal of Climatology*.

Tables:

Table 1. WRF physics parameterization options tested in model sensitivity analyses

Physics	**PH01**	**PH02**	**PH03**	**PH04**
Microphysics	WSM6	Thompson	WSM6	LIN
Radiation Physics	CAM	CAM	CAM	CAM
Land Surface Model	NOAH	NOAH	NOAH	NOAH
Planetary Boundary Layer	MYJ	MYJ	YSU	MYJ
Cumulus scheme	BMJ	BMJ	BMJ	BMJ

Table 2. Names and locations of the 12 sub-regions for analysis.

#	Name	Longitude (Degrees East)	Latitude (Degrees North)	Region
1	Tana	37.2	12.0	Lake Tana
2	GERD	34.8	11.1	Grand Ethiopian Renaissance Dam
3	HAD	32.9	23.0	High Aswan Dam
4	Khartoum	32.5	15.5	Khartoum
5	Atbara	34.4	17.5	Atbara River
6	Sobat	34.5	8.5	Sobat River
7	Merowe	32.0	18.5	Merowe Dam
8	Tekeze	38.0	14.0	Tekeze
9	Akobo	34.0	6.0	Akobo River
10	BN	39.0	10.0	Blue Nile River
11	Pibor	33.2	4.5	Pibor
12	Obeid	29.0	13.0	Obeid

Table 3. Comparison between Physics groups "1" and "4".

	Physics 1			**Physics 4**		
	RMSE	**MAE**	**COR**	**RMSE**	**MAE**	**COR**
Dry Year (1984)	0.73	1.29	0.5	0.68	1.24	0.49
Wet Year (1999)	1.0	1.15	0.47	0.96	1.09	0.5

Figures:

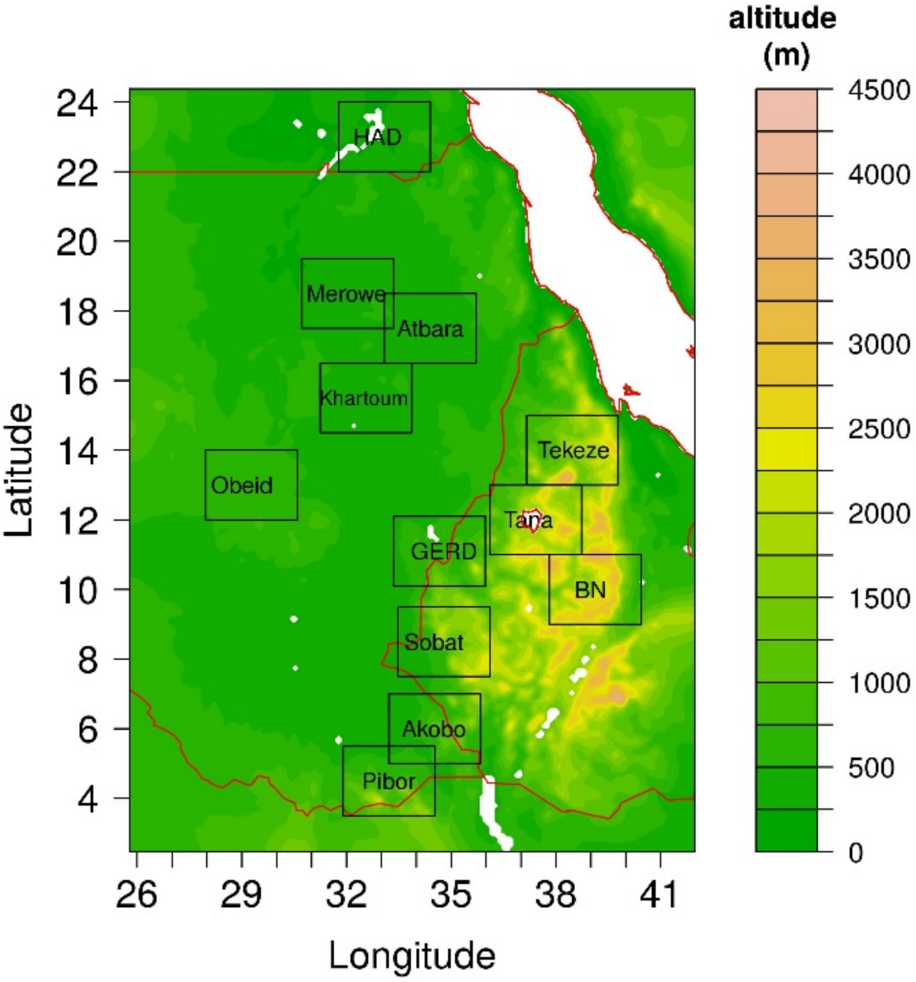

Figure 1. The Eastern Nile (EN) basin and sub-regions for evaluation

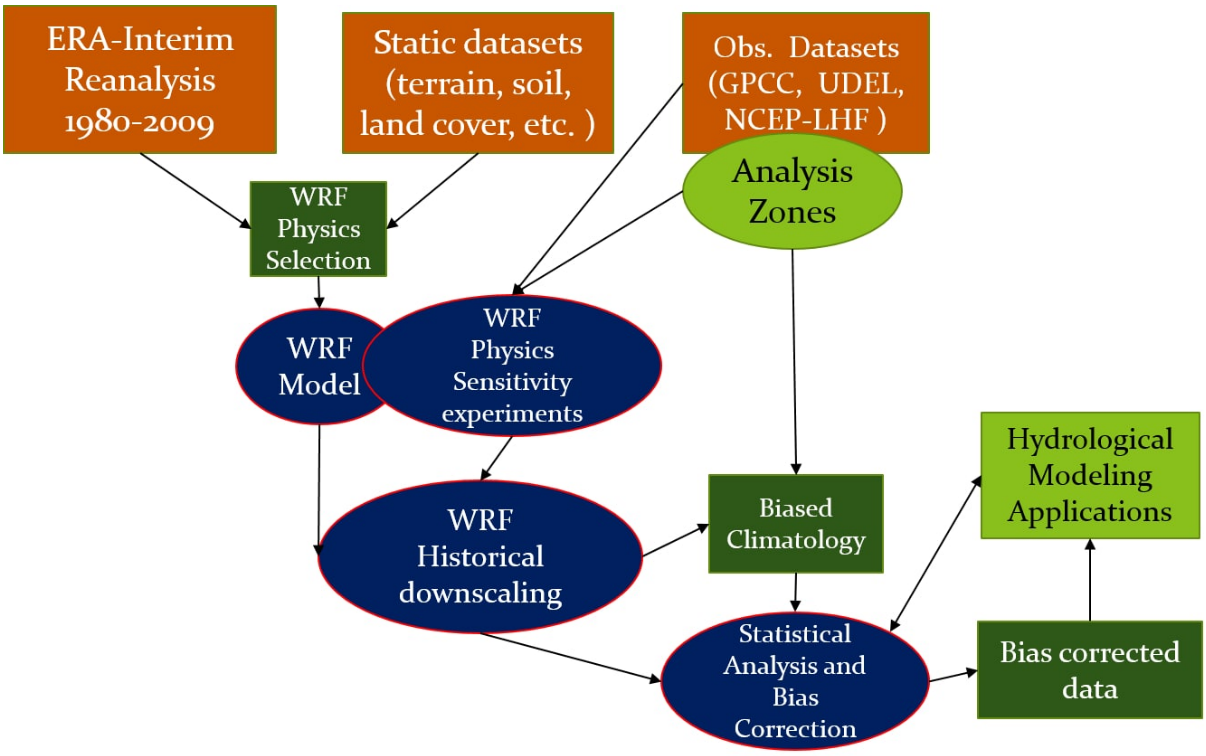

Figure 2. Methodology flow chart.

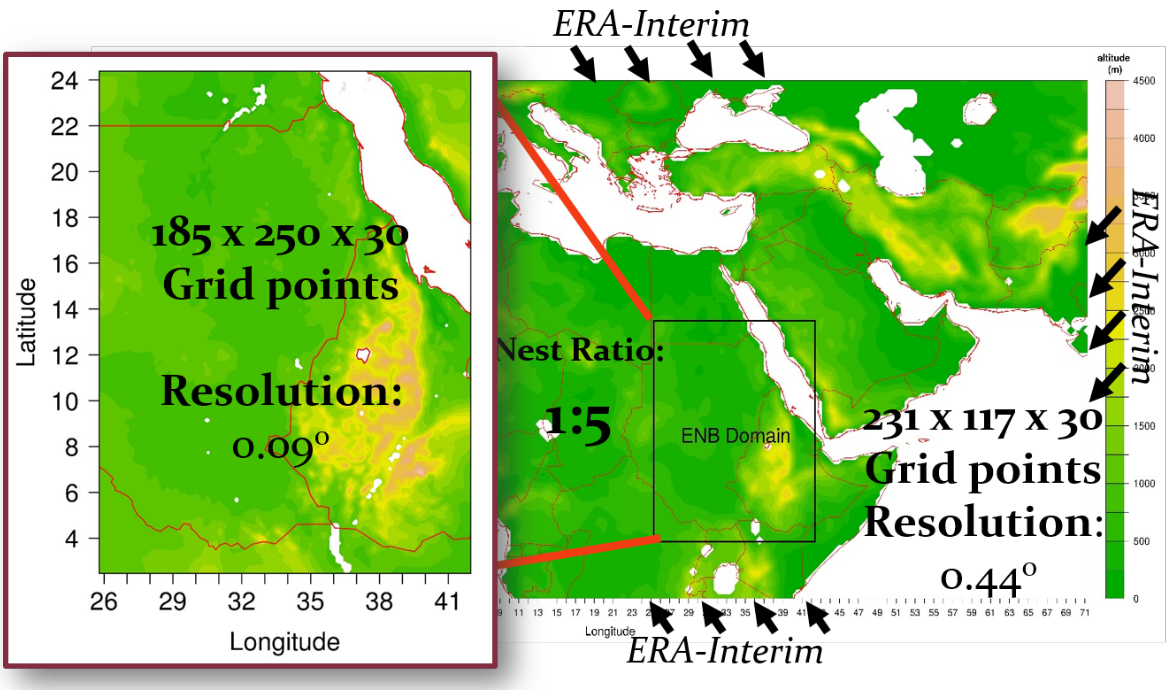

Figure 3. EN domain setup, nested within CORDEX MENA.

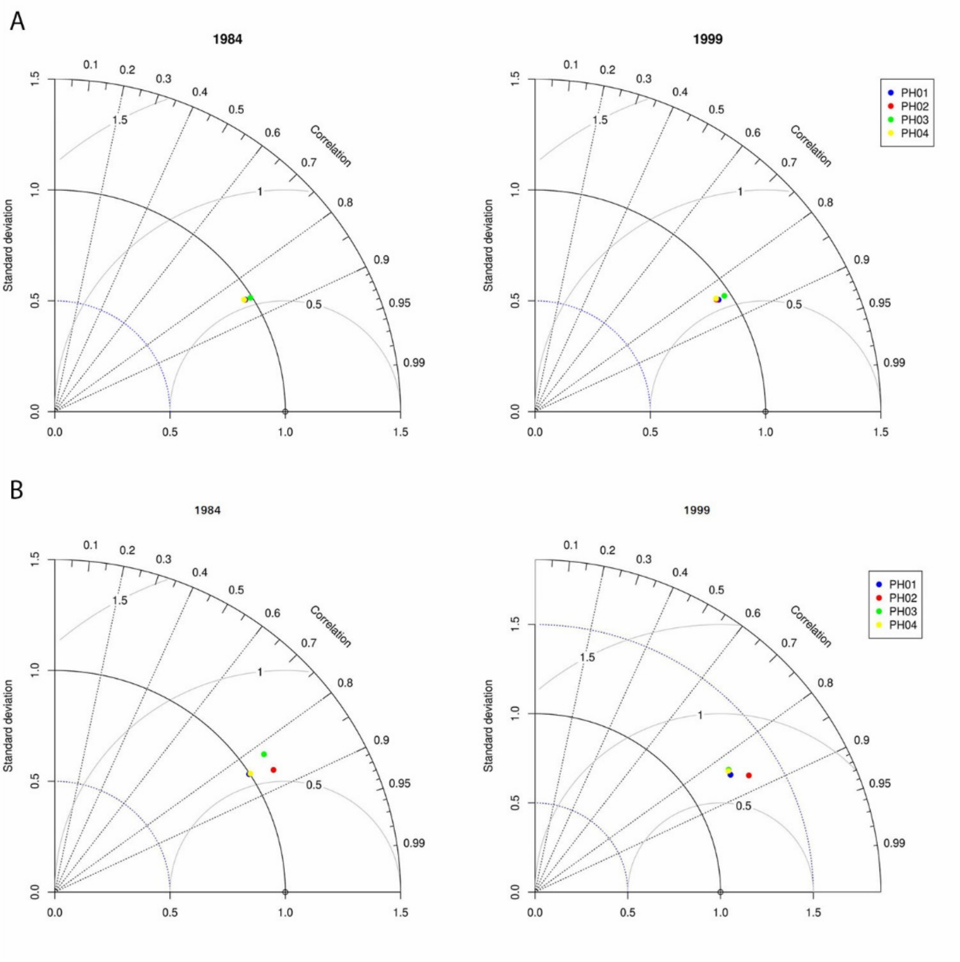

Figure 4. (A) Taylor diagram for temperature over the EN basin for the four physics groups over the two test years, 1984 and 1999. (B) Taylor diagram for precipitation over the EN basin for the four physics groups over the two test years, 1984 and 1999.

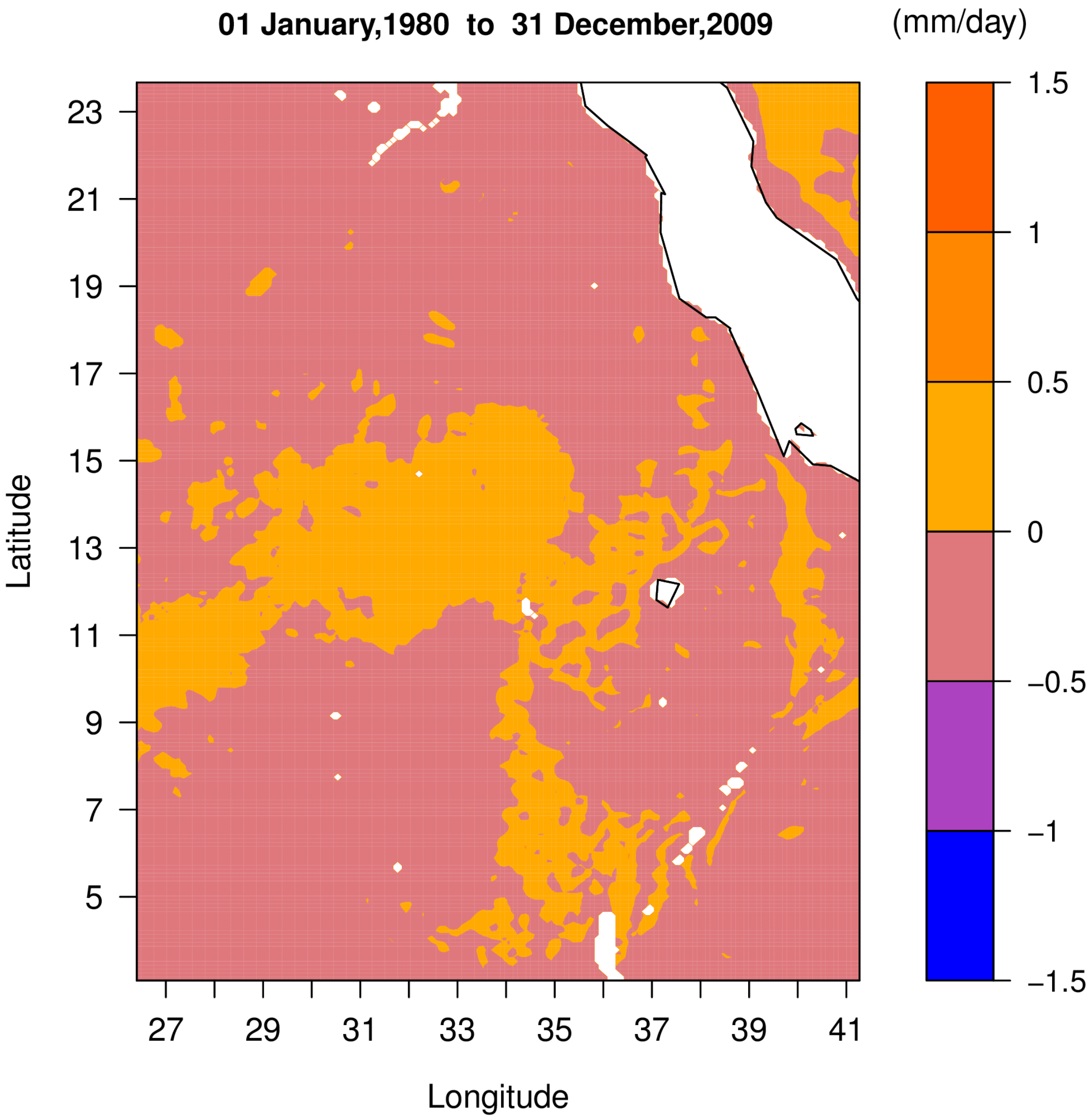

Figure 5: WRF evapotranspiration, average daily bias from the NCEP-LHF dataset between 1980 and 2009.

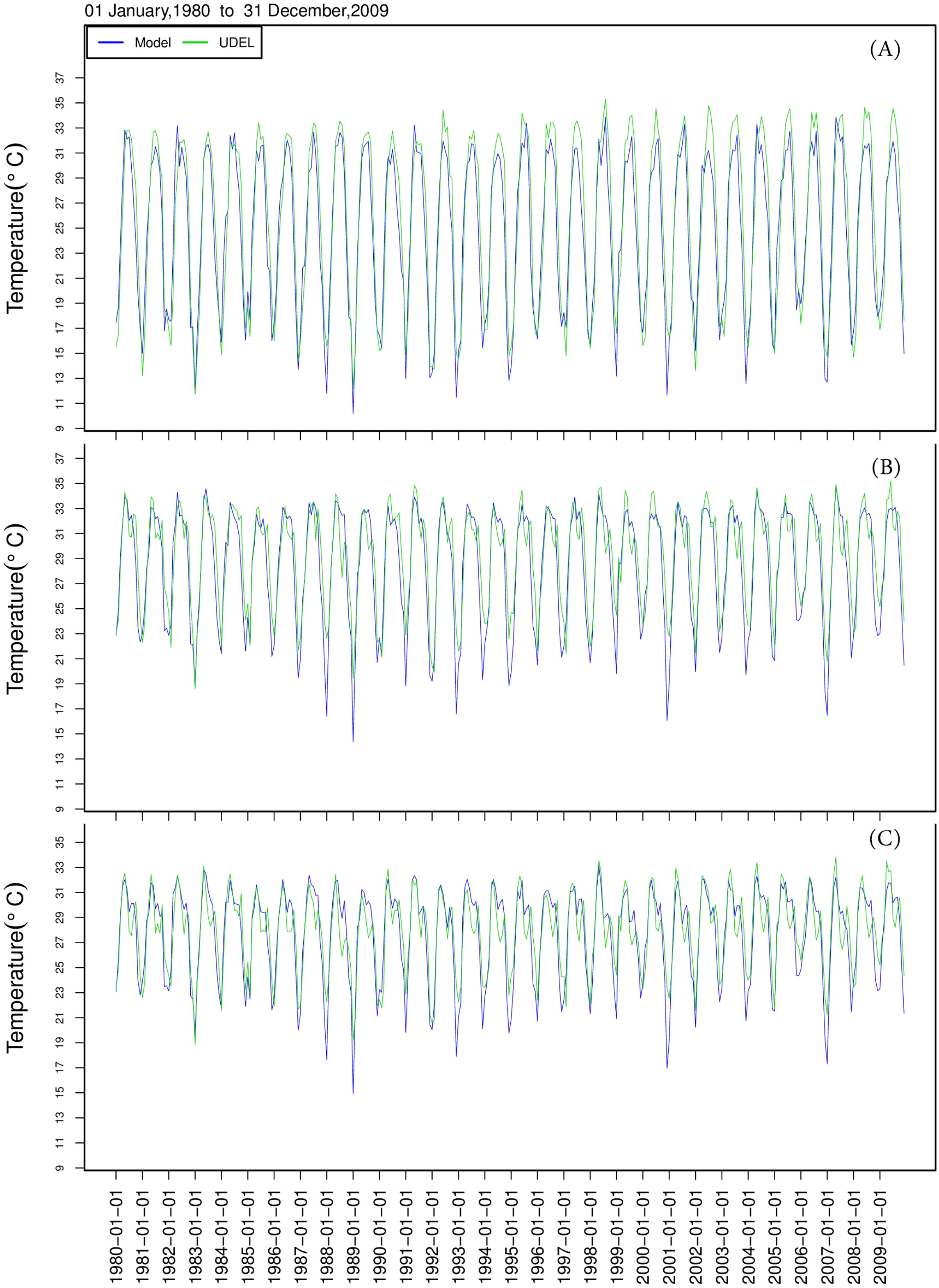

Figure 6: WRF modeled temperature time series at: (A) HAD, (B) Khartoum and (C) Obeid.

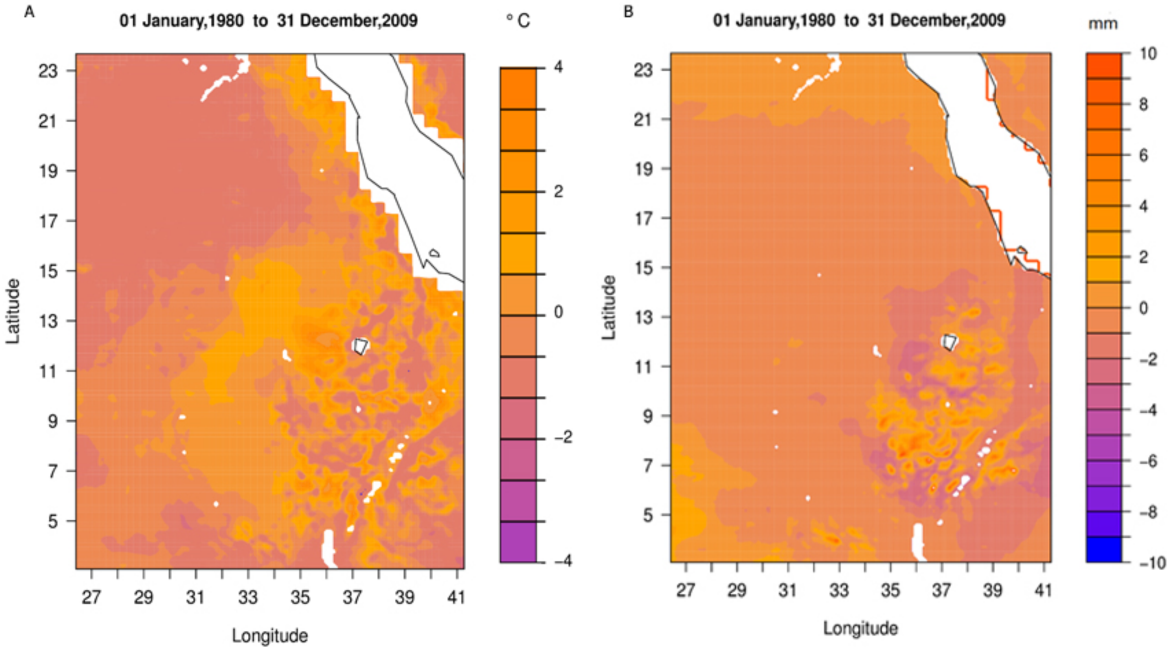

Figure 7: (A) WRF modeled temperature bias compared to UDEL. (B) WRF modeled precipitation bias compared to GPCC.

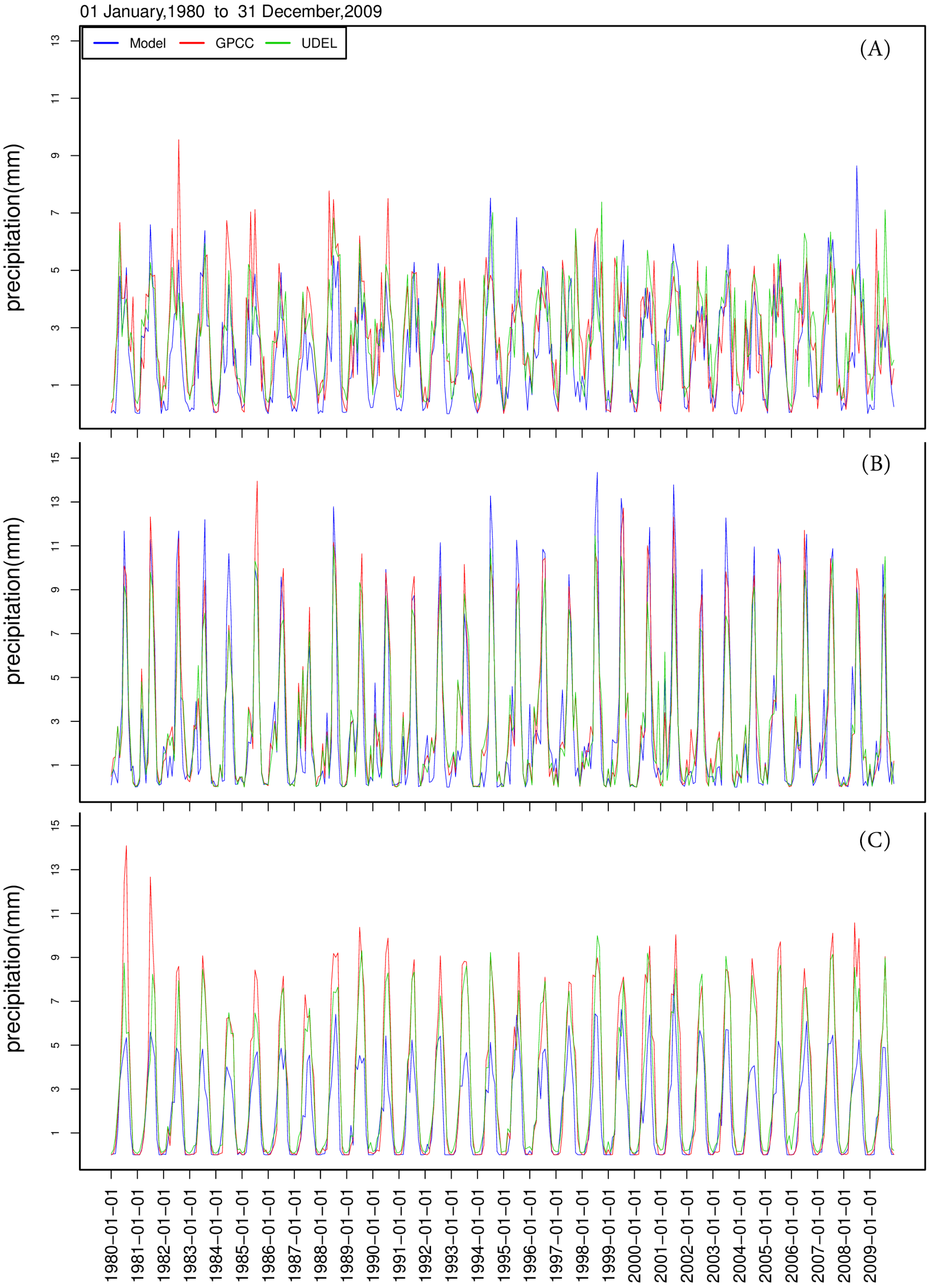

Figure 8: WRF modeled precipitation time series at: (A) Akobo, (B) BN and (C) GERD.

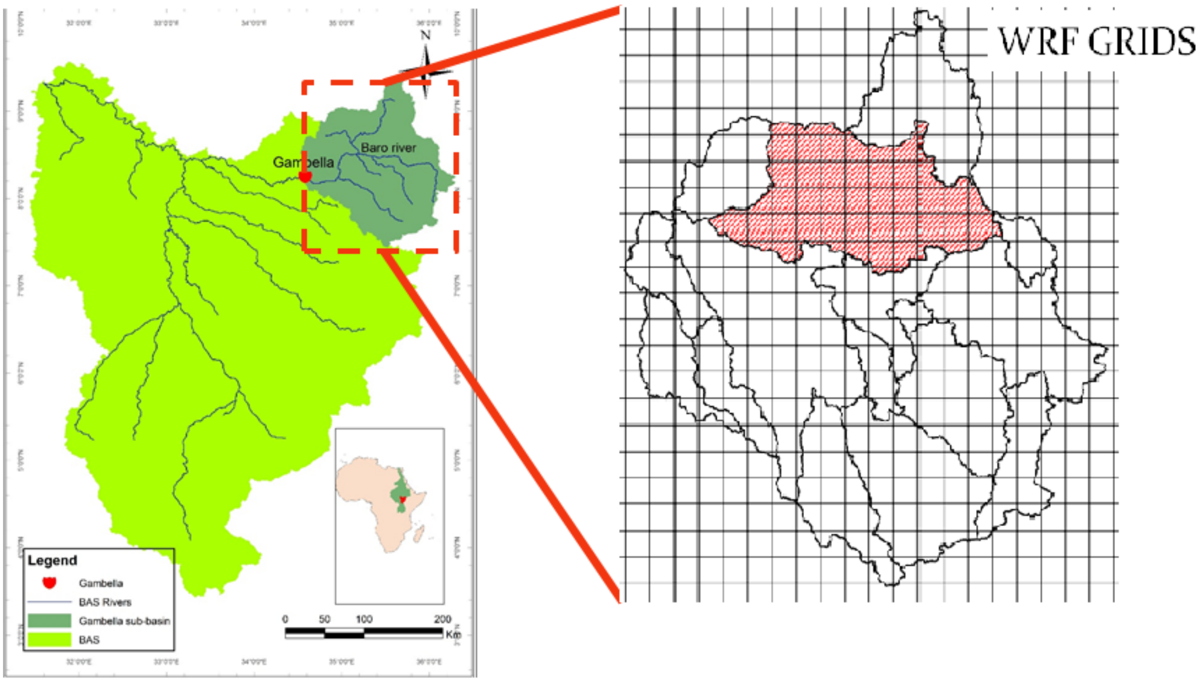

Figure 9: Gambella watershed location (left) and within the WRF model grid at a resolution of 0.09°x0.09° (right).

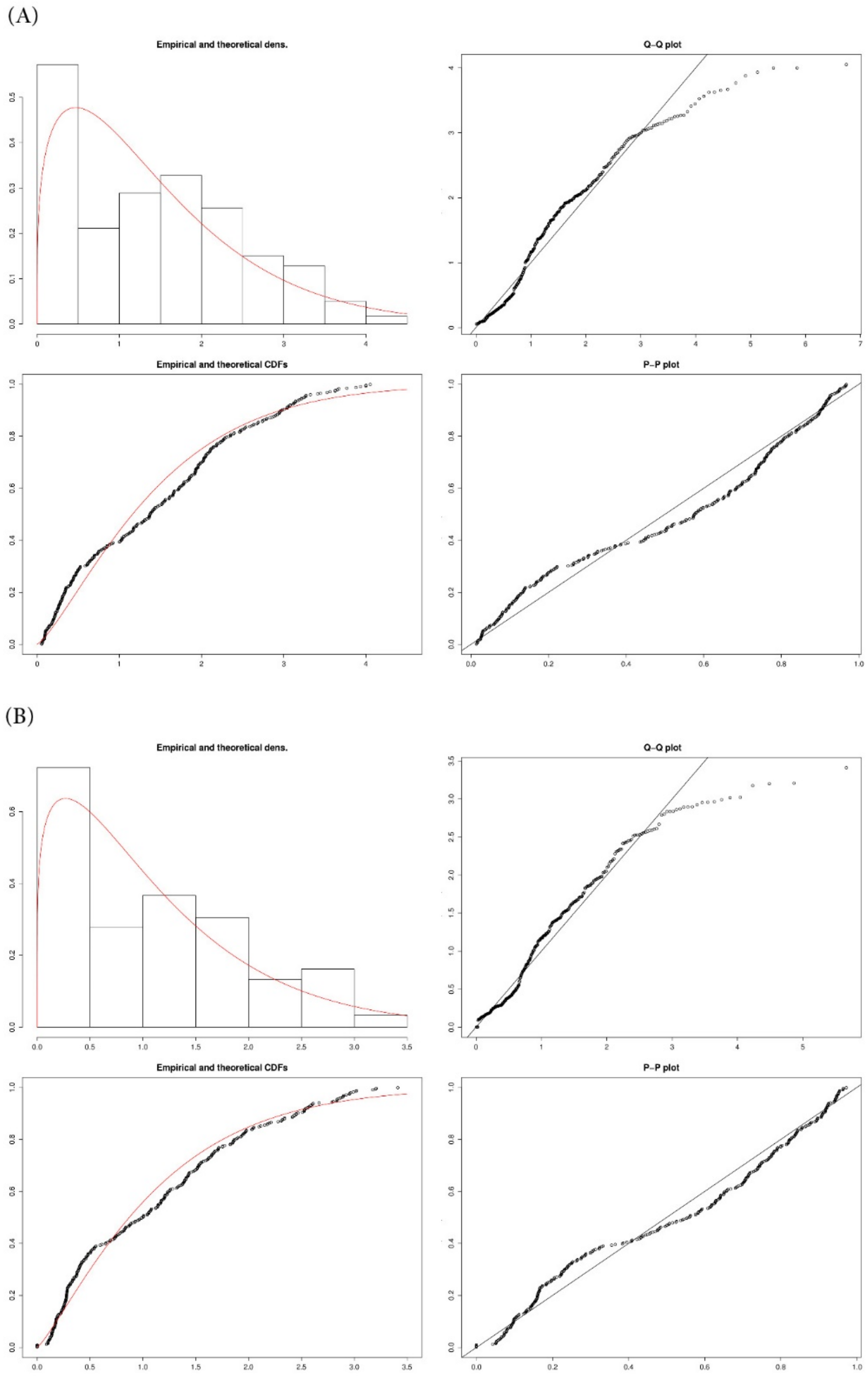

Figure 10: (A) GPCC precipitation Weibull distribution fitting. (B) WRF precipitation Weibull distribution fitting.

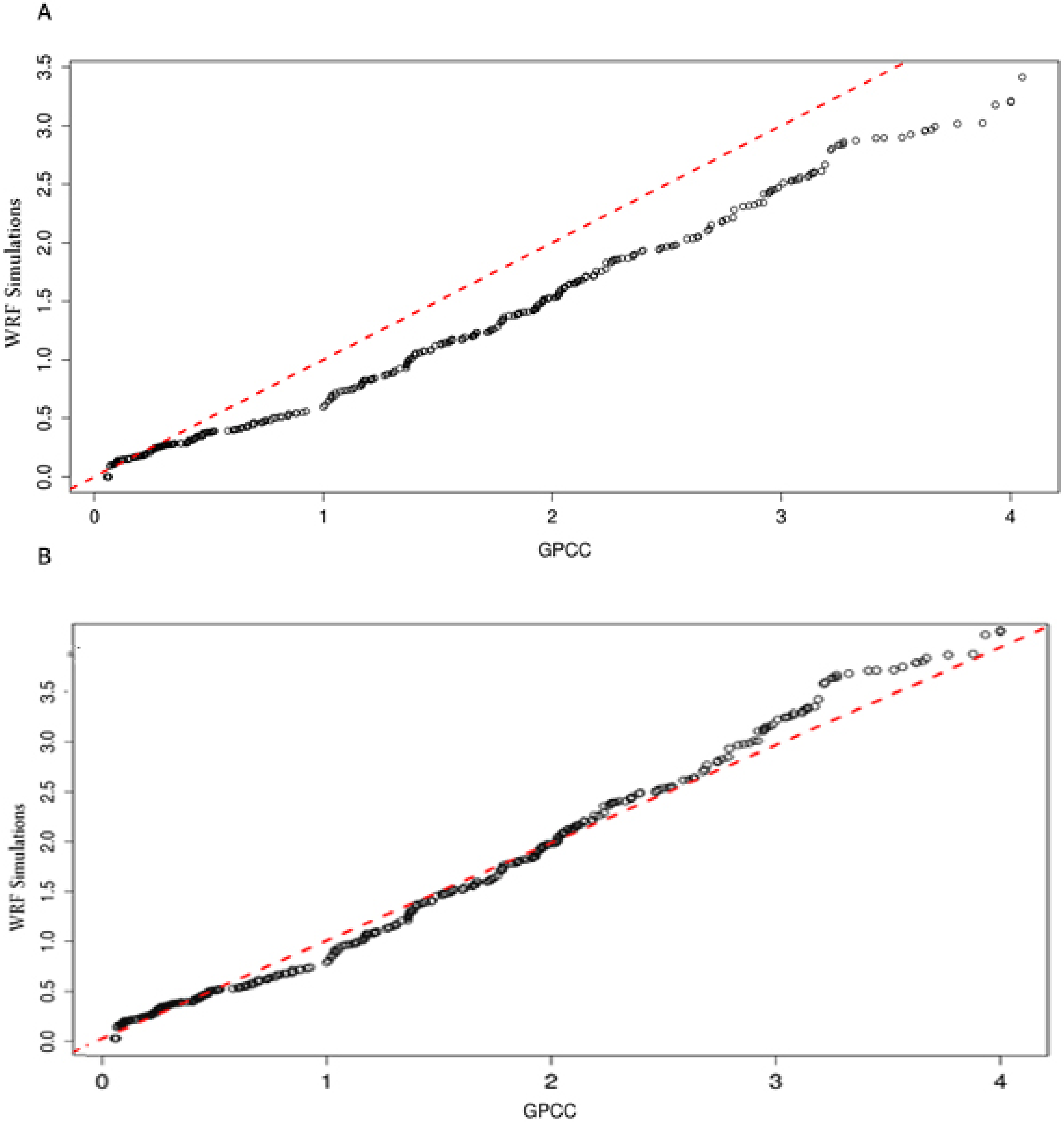

Figure 11: (A) Q-Q plot for the modeled precipitation vs. the GPCC data. (B) Q-Q plot for the bias-corrected simulated precipitation vs. the GPCC data.

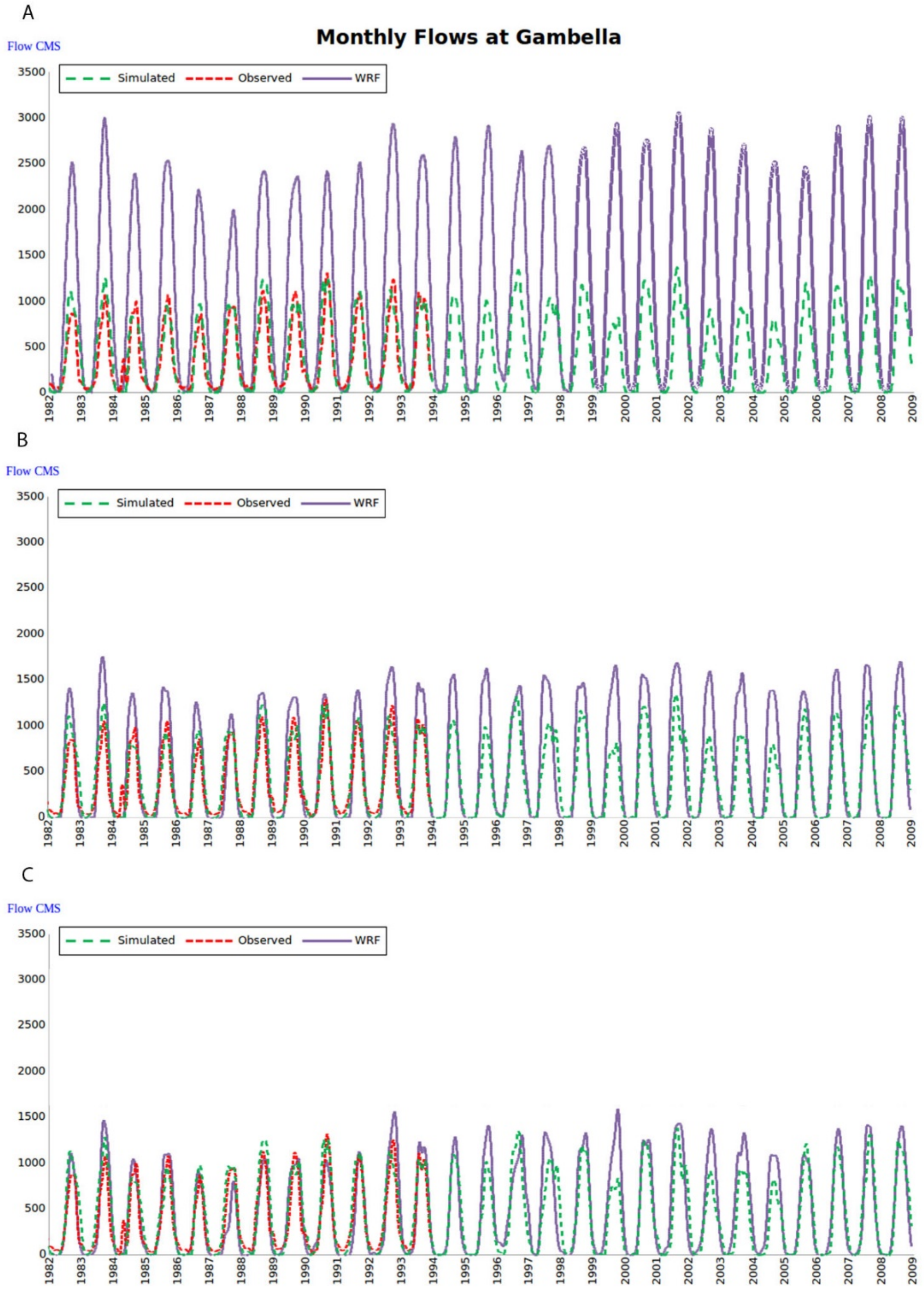

Figure 12: Comparison of monthly flow at Gambella watershed between model forced by satellite data and WRF bias corrected precipitation: (A) probability distribution corrected, (B) Elevation-location corrected, (C) Time-location corrected.

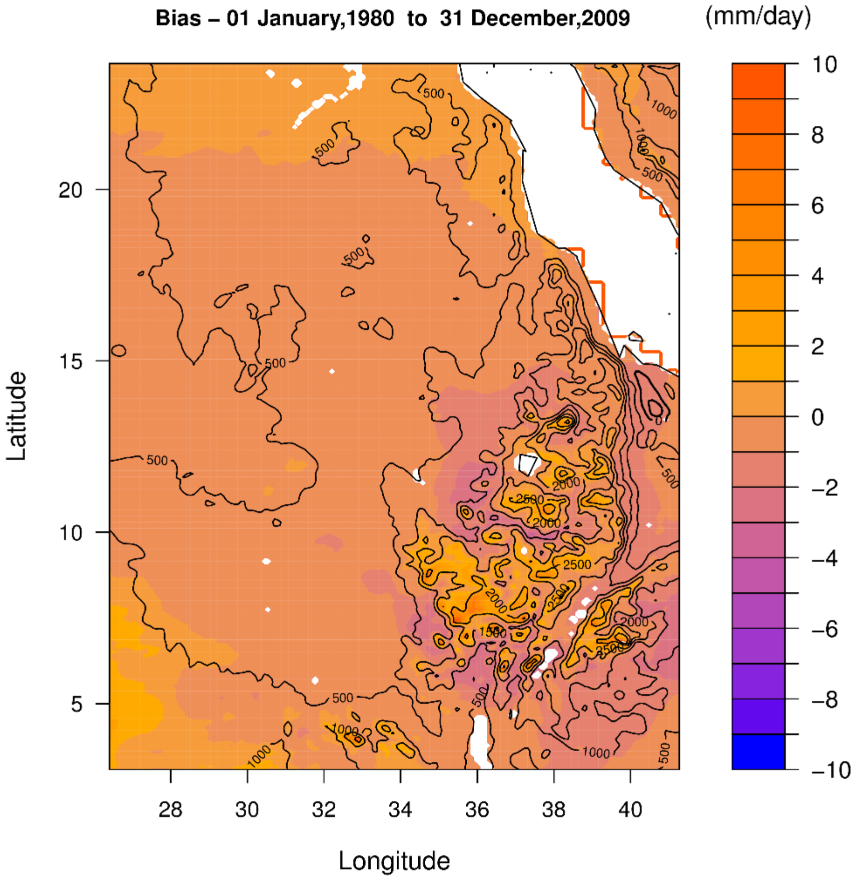

Figure 13: WRF 30-year mean precipitation bias and terrain elevation contour lines.

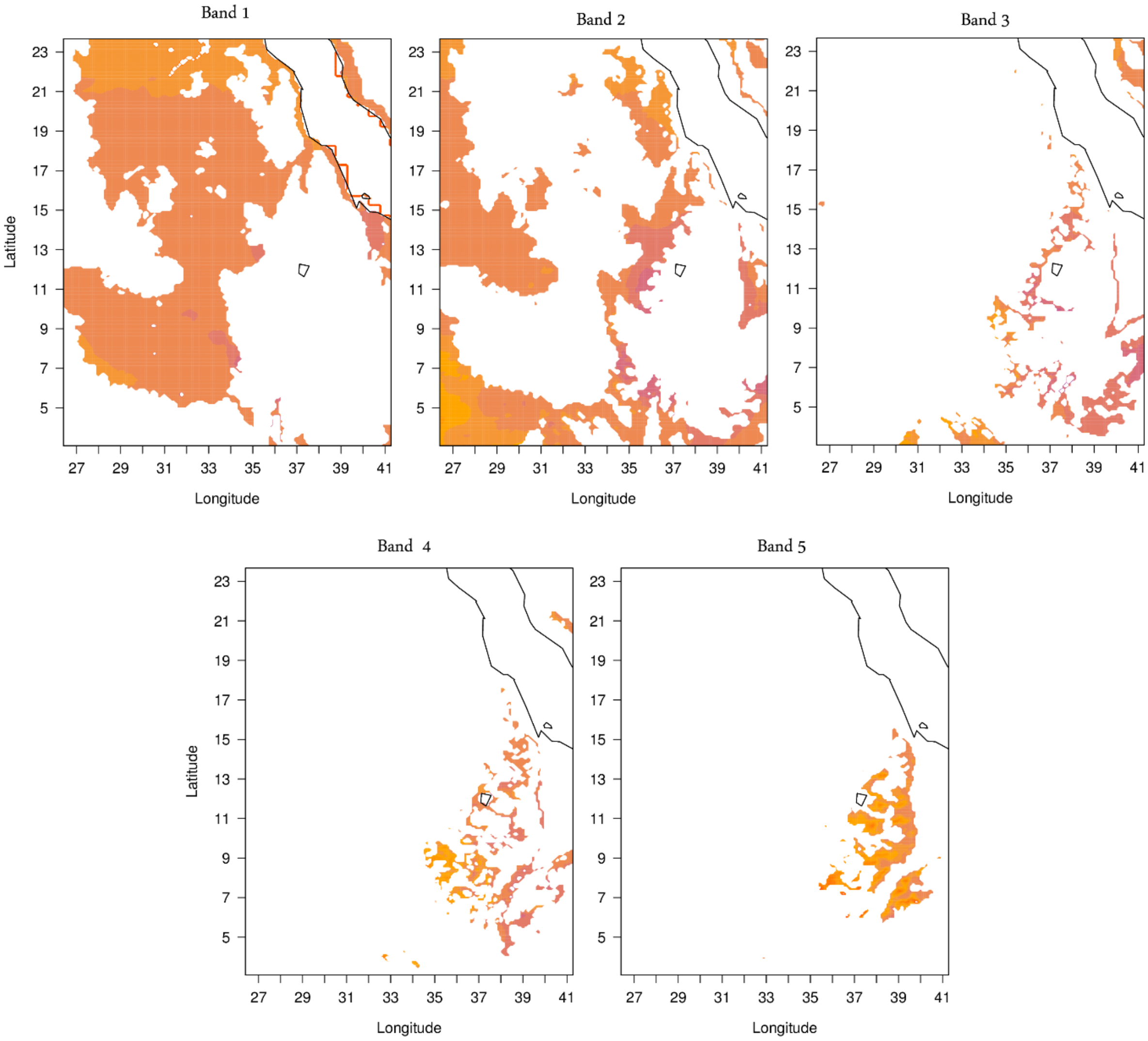

Figure 14: WRF precipitation bias in the five elevation bands.

487

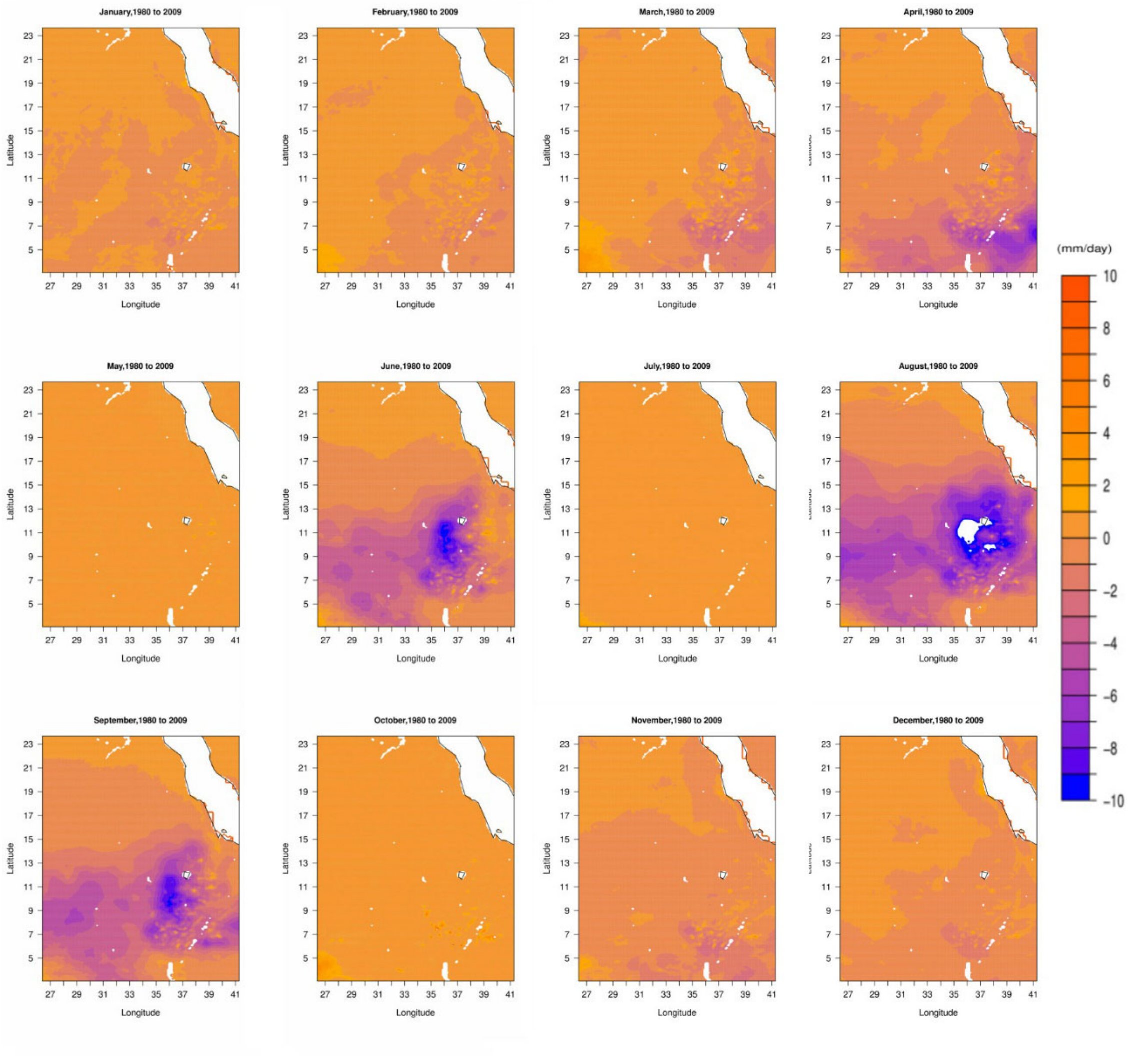

488 **Figure 15: Monthly time-location precipitation bias corrections.**